Intermittency in a stochastic parameterization of nonorographic gravity waves

A. de la Cámara, F. Lott, A. Hertzog

AGU PUBLICATIONS

JGR

Journal of Geophysical Research: Atmospheres

RESEARCH ARTICLE

10.1002/2014JD022002

Key Points:
- Importance of reproducing the observed intermittency in GW parameterizations
- Characteristics of GW intermittency arise in good part from GW sources
- Reconciliation between multiwave and globally spectral GW parameterizations

Correspondence to:
A. de la Cámara,
acamarai@lmd.ens.fr

Citation:
de la Cámara, A., F. Lott, and A. Hertzog (2014), Intermittency in a stochastic parameterization of nonorographic gravity waves, *J. Geophys. Res. Atmos.*, *119*, 11,905–11,919, doi:10.1002/2014JD022002.

Received 7 MAY 2014
Accepted 9 OCT 2014
Accepted article online 12 OCT 2014
Published online 6 NOV 2014

Intermittency in a stochastic parameterization of nonorographic gravity waves

A. de la Cámara[1], F. Lott[1], and A. Hertzog[2]

[1]Laboratoire de Météorologie Dynamique, IPSL and CNRS, École Normale Supérieure, Paris, France, [2]Laboratoire de Météorologie Dynamique, IPSL and CNRS, École Polytechnique, Palaiseau, France

Abstract A multiwave stochastic parameterization of nonorographic gravity waves (GWs), representing GWs produced by convection and a background of GWs in the midlatitudes, is tuned and tested against momentum fluxes derived from long-duration balloon flights. The tests are done offline using data sets corresponding to the Southern Ocean during the Concordiasi campaign in 2010. We also adopt the limiting constraint that the drag produced by the scheme resembles that produced by a highly tuned spectral GW parameterization, the so-called Hines scheme. Our results show that the parameterization can reproduce the momentum flux intermittency measured during the campaign, which is relevant since it strongly impacts on the vertical distribution of the GW drag. We also show that, at the altitude of the balloon flights, the momentum flux intermittency is in good part due to the GW sources: filtering by the background winds only becomes effective at much higher altitude. These results are based on bulk formulae for the GW momentum flux that could be used to replace our background GWs by GWs produced by fronts. Finally, the GW energy spectra built out of the stochastic scheme by averaging over a large ensemble of realizations are comparable to the classical vertical spectra of GWs, used today in globally spectral schemes. This indicates that multiwave and spectral schemes can be reconciled once a stochastic approach is used.

1. Introduction

Gravity waves (GWs) generated from nonorographic sources are subject of active observational [e.g., *Hertzog et al.*, 2012; *Hoffmann et al.*, 2013], theoretical [e.g., *Lott et al.*, 2010, 2012b], and modeling research [e.g., *Plougonven et al.*, 2013; *Jewtoukoff et al.*, 2013]. This interest follows that GWs are an important driver of the circulation of the middle atmosphere, contributing for instance to the quasi-biennial oscillation (QBO) forcing [*Lindzen and Holton*, 1968] and to the formation of the summer cold mesopause [e.g., *Holton*, 1983].

The spatial scales of the GWs are generally too small to be represented in global general circulation models (GCMs), and their effects on the resolved scales need to be parameterized. For this purpose, two distinct "families" of GW parameterizations have emerged over the last three decades, hereinafter called "globally spectral" and "multiwave" schemes. In the first family, parameterizations use the observational fact that GW energy spectra have well-determined slopes along, for instance, their vertical wave number, which allows to treat a large ensemble of waves at a reasonable cost via theoretical integrations [e.g., *Hines*, 1997; *Warner and McIntyre*, 1996; *Scinocca*, 2003]. In the second family, the spectral domain is binned by a large number of monochromatic waves, and the breaking of each wave is treated independently from the others [*Lindzen*, 1981; *Alexander and Dunkerton*, 1999; *Song and Chun*, 2008; *Richter et al.*, 2010]. As discussed in *Lott et al.* [2012a] and *Lott and Guez* [2013], the two approaches have arguments for and against. Recent observations showing that GWs often travel as wave packets (i.e., fluctuations at a given time and location dominated by a single GW with its particular set of wave parameters, such as amplitude, horizontal, and vertical wavelength) [e.g., *Hertzog et al.*, 2008; *Wright et al.*, 2013] justify the use of multiwave schemes. These parameterizations have the advantage of being largely based on linear wave theory where it is easy to include the convective sources (see *Lott and Guez* [2013] and equation (2) here). Recent linear theory of GWs produced by potential vorticity anomalies suggest that bulk formula linking GW fluxes and relative vorticity amplitude could also be used to represent the GWs produced by fronts at small cost (see *Lott et al.* [2010, 2012b] and section 4.2 here). Linear theory is nevertheless not well adapted to treat wave breaking far from critical levels. In this respect, the globally spectral schemes are better adapted, since they are based on systematic observations of GW energy spectra. On the other hand, they have the defect of considering that the entire spectrum of GWs is realized at each model grid point and at each time, somehow contradicting the fact

that GWs often travel in narrowbanded wave packets. For this reason, the spectral schemes are not really adapted to link the GWs to potential sources, simply because a given source at a given time and location is not supposed to launch the entire spectra of GWs. In this paper, we will show that the two approaches are not opposed, and that realistic spectra can be produced out of a stochastic multiwave scheme by averaging over a large ensemble of realizations.

A major effort has been made over recent years to constrain the tunable parameters of GW parameterizations with observations in the stratosphere [*Alexander et al.*, 2010; *Ern et al.*, 2011; *Geller et al.*, 2013; *Hoffmann et al.*, 2013]. Although parameterizations are often found to be reasonably realistic, *Geller et al.* [2013] found that agreement, or lack of it, between observed and parameterized GW momentum flux at a given altitude does not imply similar agreement on the GW drag deposited aloft. The reason is that the conditions for GW breaking depend on the model winds and temperature but also that the intermittency of the parameterized GW field has a very strong effect. A given averaged flux produced by a large number of small-amplitude waves will produce a drag at much higher altitudes than if the same averaged flux is transported by few large GWs. Today, this issue becomes central since sporadic and very intense GW events are shown in recent observations from long-duration balloon flights [*Hertzog et al.*, 2008, 2012; *Plougonven et al.*, 2008], satellite measurements [*Hertzog et al.*, 2012; *Wright et al.*, 2013], ground-based radars and airglow imager [e.g., *Fritts et al.*, 2002, 2012], and in high-resolution simulations with mesoscale models [*Hertzog et al.*, 2012; *Plougonven et al.*, 2008, 2013].

The purpose of the present paper is to show that the stochastic methods used to handle the multiwave schemes in *Eckermann* [2011], *Lott et al.* [2012a], and *Lott and Guez* [2013] are suitable to capture (i) the intermittency of the GW field, (ii) realistic GW spectra, and (iii) realistic GW drag. We further illustrate that the representation of intermittency is mandatory to parameterize the GW drag realistically and to analyze the origin of the observed intermittency. We will also show that GW intermittency comes in part from intermittency of the sources (and not only from the filtering of the GWs by the zonal mean flow as suggested by *Hertzog et al.* [2012]). To address these issues, we use the GW parameterization scheme presented by *Lott et al.* [2012a] and *Lott and Guez* [2013], which successfully helps produce a QBO in the Laboratoire de Météorologie Dynamique Zoom (LMDz) GCM. Nevertheless, in both works the stochastic parameterization was only used to represent the GWs produced by convection, whereas the waves produced within fronts in the midlatitudes were still parameterized using the globally spectral *Hines* [1997] scheme. This coexistence between two distinct GW schemes is not entirely satisfactory and only justified by practical reasons. Consequently, in the present paper we follow *Eckermann* [2011] and apply the stochastic methods to the GWs that affect the midlatitudes. For this purpose we add a stochastic background flux to the launched convective GW fluxes described by *Lott and Guez* [2013]. This scheme, which combines stochastically and convectively generated GWs, will be referred to as BCGWD. We then constrain the tunable parameters of the BCGWD scheme with observations of GW momentum flux intermittency derived from long-duration balloon flights in the lower stratosphere over the Southern Ocean during the Concordiasi field campaign in the austral spring of 2010 [*Rabier et al.*, 2010]. Offline tests of the BCGWD scheme are conducted using daily wind and temperature fields from reanalysis data sets and precipitation from global observations, all at the same $1° \times 1°$ longitude-latitude resolution. We do offline rather than online tests because we want the large-scale winds, temperature, and precipitation fields to correspond to those present when the balloon observations we use were made. In addition, *Lott and Guez* [2013] showed that offline results translate very well online in GCMs.

The remainder of the paper is organized as follows. Section 2 describes the data used for the offline tests, including a brief description of the Concordiasi balloon campaign in 2010, overviews the formalism of the GW parameterization, and specifies the scheme setup. Results of momentum flux intermittency are presented in section 3, while section 4 discusses the significance and potential causes for intermittency and presents the GW energy spectra that can be constructed out of the scheme. Finally, a summary and the main conclusions are given in section 5.

2. Data and Methods

2.1. Data

Three different databases are used in this study. The first one is in situ monitoring of the extratropical lower stratosphere by superpressure balloons launched during the Concordiasi campaign in Antarctica in the austral spring of 2010 [*Rabier et al.*, 2010]. A total number of 19 balloons successfully drifted inside the Antarctic polar vortex at a given isopycnal surface at around 20 km height from September 2010

until January 2011. The sample frequency was 1/30 Hz, which allowed to measure a large part of the GW spectrum (visit http://www.cnrm.meteo.fr/concordiasi/ for further details). In particular, we make use of the data set of GW momentum flux computed following the methodology described by *Boccara et al.* [2008] and applied by *Hertzog et al.* [2008] to the balloon data from the previous Vorcore campaign [*Hertzog et al.*, 2007].

The second data set is daily (at UTC1200) horizontal wind and temperature fields from the European Centre for Medium-Range Weather Forecasts (ECMWF) reanalysis ERA-Interim [*Dee et al.*, 2011]. The data are archived on a 1°×1° longitude-latitude grid, on 60 pressure levels spanning from 1000 hPa to 0.1 hPa. The last data set is the global precipitation field from Global Precipitation Climatology Project (GPCP) [*Adler et al.*, 2003]. We use daily data at UTC1200 on the same horizontal grid of 1°×1° as the ERA-Interim data. The data from these two sources are used as input of the parameterization.

2.2. Extension of the Convective GW Scheme to Include a Background of GWs

The GW parameterization used in the present study follows *Lott et al.* [2012a] and represents the GW field with a stochastic series:

$$w' = \sum_{n=1}^{\infty} C_n w'_n(x,y,z,t), \text{ where } w'_n = \Re\left\{\hat{w}_n(z) e^{z/2H} e^{i\left(\vec{k}_n\cdot\vec{x}-\omega_n t\right)}\right\}, \tag{1}$$

the intermittency coefficients C_n's satisfying the normalization relation $\sum_1^{\infty} C_n^2 = 1$. Following the interpretation in *Lott et al.* [2012a], C_n^2 is the probability that the wavefield is realized entirely by the nth wave, so each GW can be treated independently from the others. In equation (1), w' is the vertical component of the GW wind perturbation, $\hat{w}_n$ is the amplitude of the nth wave, $z = H\log(p_r/p)$ is the log-pressure height (where p is pressure, p_r is a reference state pressure, $H = RT_r/g$ is a scale height, R is the universal gas constant, T_r is the reference state temperature, and g is gravity acceleration), $\vec{k}$ is the horizontal wave number vector, and ω is the absolute (i.e., ground-based) frequency.

The momentum flux carried by each wave is specified at a given launching altitude z_l by

$$\vec{F}^{z_l} = \underbrace{\rho_r G_{uw0}\left(\frac{RL_W}{\rho_r H c_p}\right)^2 \frac{|\vec{\hat{k}}|^2 e^{-m^2\Delta z^2}}{N\Omega^3}\hat{P}\hat{P}^*\frac{\vec{k}}{|\vec{k}|}}_{\text{flux from convective sources}} + \underbrace{G_b(1-\gamma\cos^8\phi)\frac{\vec{k}}{|\vec{k}|}}_{\text{background flux}}, \tag{2}$$

where the n indices have been dropped for conciseness. The first term in the right-hand side of equation (2) represents the contribution from convective sources (see *Lott and Guez* [2013] for a formal derivation). The second term in the right-hand side represents the contribution from the background flux and accounts for GWs from nonconvective (and nonorographic) sources. The influence of this second term is confined to the extratropical latitudes via the factor $(1-\gamma\cos^8\phi)$, where ϕ is latitude and the factor $0 < \gamma < 1$. In equation (2), ρ_r is the reference state density, G_{uw0} is a tunable, adimensional parameter related to the flux amplitude of the convective GWs, L_W is the latent heat of condensation, m is the vertical wave number ($m^2 = N^2|\vec{k}|^2/\Omega^2$), Δz is the vertical width over which the released heating due to condensation is distributed, N is the buoyancy frequency, $\hat{P}$ is the grid precipitation, $\Omega = \omega - \vec{k}\cdot\vec{U}$ is the intrinsic frequency, and G_b is the background (nonconvective) GW flux amplitude.

To represent vertical propagation, the momentum flux is almost conserved from one level to the next in the absence of breaking or critical levels, at least in the stratosphere and lower mesosphere. In fact, we consider that a small diffusivity μ_d/ρ_0 acts on the waves to ensure that the flux is dissipated over the last few model levels (this is ensured by the density in the denominator; see equation (3)). Besides, the GW momentum flux is limited by that produced by a saturated monochromatic wave [e.g., *Lindzen*, 1981], and the flux is set to zero where the waves encounter a critical level. The passage of Eliassen-Palm (E-P) flux from one level to the next (equation (12) by *Lott and Guez* [2013]) can be written as

$$\vec{F}^z(z+\delta z) = \frac{\vec{k}\Omega}{|\vec{k}||\Omega|}\Theta(\Omega(z+\delta z)\Omega(z))\min\left\{|\vec{F}^z(z)|e^{-2\frac{\mu_d m^3}{\rho_0\Omega}\delta z},\ \rho_r S_c^2\frac{|\Omega|^3 k_{\min}^2}{N|\vec{k}|^4}\right\}, \tag{3}$$

where the Heaviside function Θ handles critical levels, S_c is a tunable parameter controlling the saturated momentum flux, and $k_{\min}$ is a minimum horizontal wave number associated with the smallest unresolved grid scale.

2.3. GW Scheme Parameters

The values of the tunable parameters are carefully chosen in order to produce GW momentum flux intermittency that compares well with the balloons measurements over oceanic areas. To this aim, we use the observational fact that the probability density functions (pdfs) of GW momentum flux from balloons and satellite measurements in the extratropics over flat terrain (i.e., nonorographic case) present a lognormal distribution at 20 km [*Hertzog et al.*, 2012]. Therefore, the variable that controls the background flux amplitude at the launching level, G_b in equation (2), is randomly chosen out of a lognormal distribution with mean 10.35 mPa and standard deviation 18.54 mPa (these values are chosen to give results consistent with observations, they correspond to a lognormal distribution with parameters $\Lambda(\mu = 1.6, \sigma = 1.2)$). Besides, as this background flux is meant to represent the GWs forced within midlatitude fronts, we take $\gamma = 0.9$ in equation (2). This choice reduces the background flux by 90% at the equator, by 50% at 22° latitude, and does not affect it poleward of 60°. For the parameters controlling the convective GWs, the choices are almost as in *Lott and Guez* [2013], with $G_{uw0} = 0.8$ for the parameter controlling the convective flux amplitude, $\Delta z = 1$ km, and $\mu_d = 1$ kg m^{-1} s^{-1} for the diffusion parameter. In opposition to the background fluxes, these settings for the convective GWs do not follow an imposed latitudinal shape. For them, the latitudinal variations will be naturally related to the variations in the precipitation climatology.

Apart from these separate treatments of the parameters controlling the launched fluxes, the convective and background waves are treated on the same footing; e.g., a given wave can have part of its amplitude coming from the background and another part from precipitation (see equation (2)). Accordingly, the parameter controlling the saturated flux only has one value $S_c = 0.4$. Also, the horizontal wave number is randomly chosen within the interval $k_{\min} \leq |\vec{k}| \leq k_{\max}$, with $k_{\max} = 10^{-3}$ m^{-1} and $k_{\min} = 1/\sqrt{\Delta x \Delta y}$ is related to the grid dimensions Δx and Δy, which in the present study correspond to a grid of 1°×1° longitude-latitude. Only waves propagating in the four cardinal directions (i.e., north, south, east, and west) are allowed. Also, we launch two pairs of waves ($M = 4$) each time step (i.e., 1 day), which means that in equation (1) $C_n^2 = 0.25$ when $n = 1, \ldots, 4$ and $C_n = 0$ otherwise, and in each pair the waves have identical wave number and amplitude but exactly opposite phase speed. This offline setup has to be distinguished from an online setup, where about the same number of waves are launched every 30 min typically. We will not discuss further this difference since we already know that offline settings translate well online essentially because the GWs are treated independently from the others regardless of their number. Finally, we choose a launching altitude in the midtroposphere ($z_l = 5$ km), and the amplitude of the absolute phase speed c is chosen from a Gaussian distribution with zero mean and a standard deviation of 40 m s^{-1}.

2.4. Gravity Wave Drag

Although the central point of our paper is to benefit from recent observations of GW momentum fluxes and their intermittency, we have to keep in mind that the information provided needs to be ultimately used online in GCMs. Here we do not make such online experiments, but we verify that the scheme predicts a GW drag comparable to that given by operational schemes. For the QBO region in the tropical stratosphere, the results are almost as in *Lott and Guez* [2013] (not shown). For the extratropical stratosphere, where the background flux makes a large contribution to the total GW momentum flux, comparisons are made with the *Hines* [1997] parameterization keeping the setup used operationally in the LMDz GCM [*Lott et al.*, 2005]. Figure 1 displays the zonal mean zonal wind tendencies (shaded) averaged over July 2010, predicted by the BCGWD parameterization (Figure 1a) and by the Hines scheme alone (Figure 1b), along with the zonal mean zonal wind from ERA-Interim (contours). The tendencies predicted by the two schemes are very similar in the upper stratosphere, characterized by a substantial deceleration in absolute terms of the zonal mean flow in both the winter and summer hemispheres. These tendencies also compare well with those provided by a high-resolution GCM that is able to resolve a large part of the GW spectrum [*Watanabe et al.*, 2008] (not shown). There are nevertheless some differences between Figures 1a and 1b. The tendencies given by the Hines scheme are more confined to the upper levels, whereas those given by the BCGWD scheme reach lower altitudes in the stratosphere. Also, in Figure 1a maxima in the summer stratosphere are located in the subtropics, which could be potentially beneficial since we know that the Hines scheme in the LMDz model underestimates the drag in this region [*Lott et al.*, 2005].

3. Intermittency of Gravity Wave Momentum Flux

To evaluate the intermittency of the GW momentum fluxes predicted by the scheme, we next analyze the pdfs of their absolute values. More specifically, we sort the values of momentum flux in bins of 1 mPa wide, a

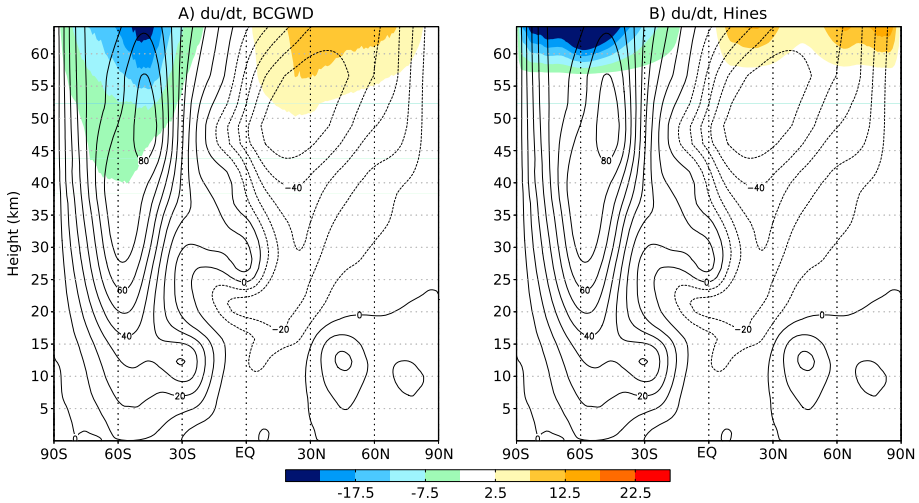

Figure 1. Zonal and temporal mean values of the nonorographic gravity wave drag (in m/s/d, shaded) and the ERA-Interim zonal mean zonal wind (in m/s, solid and dashed lines) for July 2010.

resolution representative of those used in observational studies, and construct histograms. The regions and time intervals over which the pdfs are constructed will be specified in the text.

3.1. Comparison With Concordiasi Observations

Figure 2 displays the pdf of GW absolute momentum fluxes obtained from the balloon observations (dark gray), together with the corresponding pdf obtained from the offline test at 20 km (black). The pdfs have been constructed in the 65°S–50°S latitude band. To compare with our nonorographic scheme, observations corresponding to GWs produced by the Antarctic Peninsula have been removed. This is done using a simple geographic criterion that excludes the Peninsula itself and its downwind wake where higher wave activity is observed. Typically, all observations between 45°W and 75°W are excluded from the balloon pdf. The different sampling of the two data sets should be noticed. For the parameterization, we have used data from all the grid points of the selected region from September 2010 to January 2011, whereas for the balloons we have taken the data corresponding to specific moments when the balloons were located in the target region over the ocean.

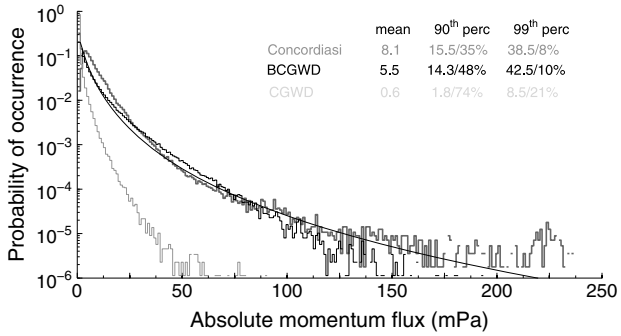

Figure 2. Pdfs (histogram style) of absolute momentum fluxes obtained with balloon observations (dark gray), and offline tests with the BCGWD (black) and CGWD (light gray, see text) configuration of the scheme at 20 km, between 65°S and 50°S during the whole Concordiasi period (September 2010 to January 2011). The continuous black line shows the pdf of a lognormal distribution with the same geometric mean and standard deviation as the BCGWD distribution. For each distribution, the (arithmetic) mean and 90th and 99th percentiles are displayed (in mPa). The percentages of total flux associated with fluxes larger than the percentiles are also indicated: for instance, in the BCGWD test, fluxes larger than 14.3 mPa occur 10% of the time (90th percentile) but correspond to the 48% of the total absolute momentum flux.

With these limitations in mind, we see in Figure 2 that the GW momentum flux distribution obtained from BCGWD resembles the observed one. Importantly, the pdfs are positively skewed and present long tails, in agreement with *Hertzog et al.* [2012] using momentum flux pdfs derived from both balloons during the Vorcore campaign in 2005 and High-Resolution Dynamics Limb Sounder (HIRDLS) measurements. Waves with small fluxes are much more likely than those with large fluxes. The 90th and 99th percentiles of the distributions are very similar between the scheme and the balloons (see percentiles in Figure 2), and the percentage of the flux they

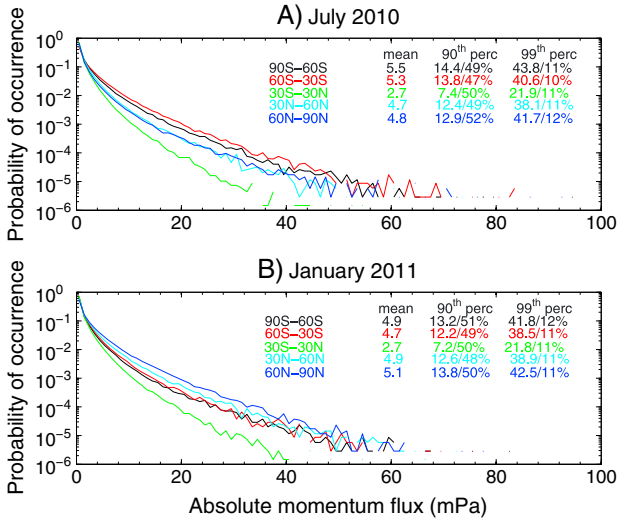

Figure 3. Pdfs of absolute momentum fluxes at 20 km obtained with offline tests of the BCGWD scheme for (a) July 2010 and (b) January 2011 and for different latitude bands as indicated.

represent is only slightly higher in the scheme (48% versus 35% in the balloons, for the 90th percentile). The largest differences between both pdfs arise at large momentum flux values (>100 mPa), with balloons observing larger fluxes than those produced by the GW scheme at 20 km. Nevertheless, the observations that few events carry significantly high GW momentum fluxes is qualitatively well captured by our stochastic parameterization.

Provided that momentum flux distributions from both balloon and satellite observations adjust to a lognormal [*Baumgaertner and McDonald*, 2007; *Hertzog et al.*, 2012], Figure 2 also displays a theoretical lognormal pdf $\Lambda(\mu, \sigma)$ with the same geometric mean e^{μ} and standard deviation e^{σ} as those of the BCGWD pdf. This lognormal pdf fairly fits that predicted by the parameterization but overestimates the occurrence of fluxes larger than 100 mPa. In contrast, the lognormal pdf derived from the GW scheme seems to better fit with Concordiasi observations in this range of large and rare momentum flux events (i.e., >100 mPa).

For illustrating purposes, we also include in Figure 2 the pdf obtained running the convective GW scheme alone (i.e., taking $G_b = 0$ in equation (2) and referred to as CGWD, light gray). In this case, the distribution also exhibits a large degree of intermittency, but clearly the mean absolute momentum flux (0.6 mPa) is much lower than that measured by the balloons (8.1 mPa). This justifies a posteriori our choice of adding a background flux active at middle-high latitudes to the GW flux produced by convection.

3.2. Variations With Latitude, Height, and Season

We next analyze the momentum flux pdfs produced by the scheme in other regions, altitudes, and seasons. We have divided the globe into five latitude bands: southern high latitudes (90°S–60°S), southern midlatitudes (60°S–30°S), tropics (30°S–30°N), northern midlatitudes (30°N–60°N), and northern high latitudes (60°N–90°N).

Figure 3 shows the pdfs at 20 km for each region, in July 2010 and January 2011. The mean fluxes in the extratropics are almost twice as large as in the tropics (5 mPa versus 2.7 mPa), with some seasonal variations. This ratio between midlatitudes and tropics is consistent with balloon observations: *Jewtoukoff et al.* [2013] have shown mean values between 3.9 and 5.4 mPa for two balloons flying in the lower tropical stratosphere, whereas during Concordiasi, observations over the Southern Ocean show a mean value of 8.1 mPa (Figure 2). Besides, the pdfs in middle-to-high latitudes present longer tails than in the tropics. Consequently, our parameterization provides more frequent events of larger fluxes in the former than in the latter region. Although this might be an artifact of our scheme since the launching flux in the extratropics has an important contribution from the background term (i.e., not related to sources), it is in good qualitative agreement with momentum fluxes derived from satellite [*Wright et al.*, 2013] and balloon observations again [*Hertzog et al.*, 2012; *Jewtoukoff et al.*, 2013]. In contrast, the percentage of the total flux associated to fluxes larger than the 90th and 99th percentiles (around 50% and 10%, respectively) remains unaltered among the various regions, including the tropics.

Regarding the seasonal modulation, no significant variations appear in the tropics, with similar pdfs, mean flux, and percentile values in July 2010 and January 2011. In the extratropics, some differences arise between summer and winter. In the winter hemisphere the distributions present longer tails than in summer for any given latitude band in the extratropics, especially in the Southern Hemisphere. Along with it, mean flux and percentiles are slightly higher in winter than in summer, with variations in the mean flux ranging

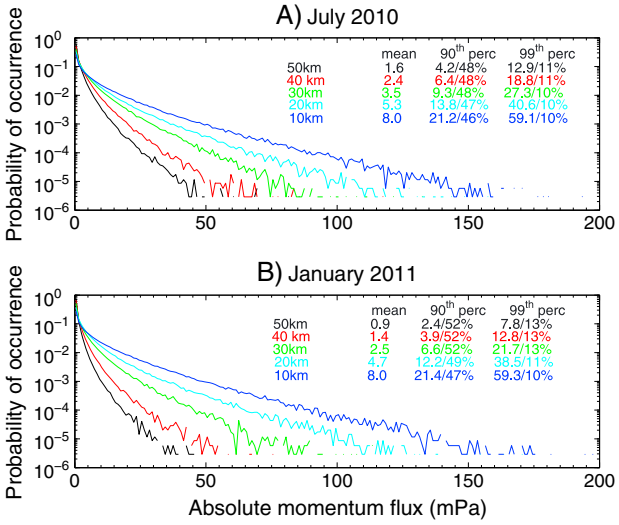

Figure 4. As in Figure 2 but for the 60°S–30°S latitude band at various heights, as indicated.

from 5% to 11%. These differences can be understood in terms of dynamical filtering by the large-scale winds. As mentioned above, the scheme launches GWs from 5 km height with phase speeds following a Gaussian distribution with mean 0 m s^{-1} and standard deviation 40 m s^{-1}. This is to say that ~60% of the waves have phase speeds $|c| \leq 40$ m s^{-1}. Since the positive zonal winds are stronger in winter than in summer between 5 and 20 km, more waves will have smaller amplitude intrinsic phase speed and hence larger amplitude vertical wave number ($|m|$) in summer. These waves are more likely to break and/or reach a critical level (the limit $|m| \rightarrow \infty$) yielding a stronger reduction of GW momentum flux between 5 and 20 km in summer than in winter. Using similar arguments, the stronger winds during the austral than during the boreal winter can in part explain the fact that a marginally larger amount of momentum flux reaches 20 km height in the southern winter than in the northern winter. Nevertheless, these seasonal differences seen in the amplitudes and pdfs of momentum fluxes reaching 20 km do not affect the momentum flux intermittency. If we evaluate it as the flux associated to the 90th and 99th percentiles, intermittency stays unaltered around 50% and 10% of the total flux, respectively.

In Figure 4 we focus on variations with altitude. For simplicity, we just show the pdfs at 10, 20, 30, 40, and 50 km height for the southern midlatitudes (60°S–30°S), but we have verified that the results are qualitatively similar in the other latitude bands (not shown). The parameterization produces momentum flux distributions with longer tails at 10 km than at any other height in any given latitude band. The pdfs at 10 km are almost identical in July and January (Figures 4a and 4b, respectively). Thus, we interpret that seasonal variations of midlatitude precipitation do not strongly affect the momentum flux at this level, maybe due to a dominant role of the background component of the launched flux in the current setup of the scheme. As we go up in the atmosphere, the momentum fluxes regularly decrease due to a combination of critical level filtering and GW breaking (i.e., wave saturation). Unlike the pdfs at 10 km, we see significant changes with season at higher altitudes. Specifically, the momentum flux reduction with height is more intense in summer than in winter (mean fluxes at 50 km of 1.6 mPa in winter and 0.9 mPa in summer), which can be understood using the same arguments of critical level filtering given above. Interestingly, the evolution with height of the pdfs in both seasons maintains the proportions between mean and percentiles: the 90th and 99th percentiles consistently correspond to around 2.5 and 8 times the distributions mean, respectively. This characteristic was also found by *Hertzog et al.* [2012] in high-resolution numerical simulations, with slightly different proportions.

3.3. Consistency With Previous Observational Studies

In the extratropics, the momentum flux pdfs variations with latitude, height, and season provided by our offline tests qualitatively agree with global satellite observations reported by *Wright et al.* [2013]. There are quantitative differences nevertheless. The seasonal variations of the pdfs and mean momentum fluxes are much weaker in the BCGWD than in observations [*Geller et al.*, 2013; *Wright et al.*, 2013]. This follows that we are launching waves with quite large phase speeds, and which are therefore less sensitive to the dynamical filtering (i.e., an important source of GW seasonal variability). We have verified that reducing the phase speeds of the waves in the parameterization strengthens the seasonal cycle of the momentum fluxes (not shown). We have not kept such a configuration because we ultimately want the new scheme to replace the Hines scheme in the LMDz GCM, which has been highly tuned online, and the configuration we adopt is consistent with the fact that the Hines scheme version we use also have a weak annual cycle. Besides, it

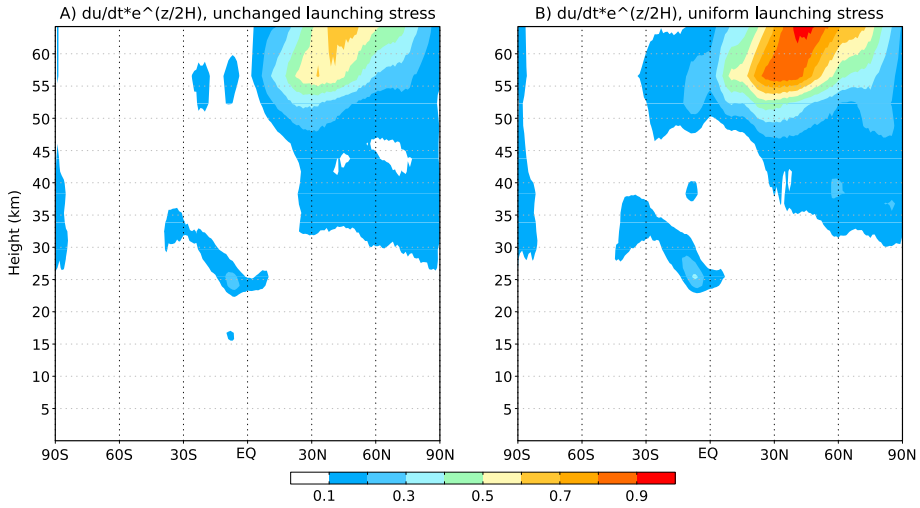

Figure 5. GW drag due to waves with positive phase speed, for July 2010. (a) GW drag and (b) GW drag when the launching momentum flux is averaged in longitude and time and zonally redistributed. The tendencies are scaled by $e^{-z/2H}$ to display on the same panel the tendencies acting at different altitudes.

is important to remark that the seasonal cycle of the extratropical mean momentum flux in the BCGWD is similar to those shown by some of the GW schemes analyzed in *Geller et al.* [2013].

In the tropics, the pdfs of GW momentum flux provided by our offline runs have similarities with those derived from satellite instruments at 25 km by *Ern et al.* [2014] and from long-duration balloon flights at 20 km during the tropical pre-Concordiasi campaign in 2010 [*Jewtoukoff et al.*, 2013]. For example, these studies present probabilities of occurrence around 10^{-2} and 10^{-3} of momentum flux events with 5 and 10 mPa, respectively, similarly to our results in Figure 3. This is an interesting agreement since events of less than 10–15 mPa are able to drive the observed QBO [*Ern et al.*, 2014], as confirmed by *Lott and Guez* [2013] who simulated a realistic QBO in the LMDz GCM with the convective part of the BCGWD scheme used here.

Regarding the differences between the tropics and the extratropics, the validations are less evident since observations somehow contradict. If we consider the quantitative measure of intermittency given by the Gini coefficients and percentiles, the satellite-derived products show that the GW fluxes are less intermittent in the tropics than in the extratropics [*Wright et al.*, 2013; *Ern et al.*, 2014], whereas in situ balloon observations show the opposite (see the analysis of the tropical pre-Concordiasi campaign and of the extratropical Vorcore campaign in *Jewtoukoff et al.* [2013] and *Hertzog et al.* [2012], respectively). For this reason we have not given much emphasis to the tropical/extratropical contrasts, and the percentiles predicted by the BCGWD are about the same in these sectors. Of course, this will probably call for further analysis and tests in the future, but today it is quite difficult to make a choice. The apparent homogeneity of the satellite data pledge in their favor, but they have limitations nowadays. As an example, the data used in *Wright et al.* [2013] and *Ern et al.* [2014] come from polar orbiting satellites, with trajectories almost perpendicular to the zonal direction at the equator. This could lead to an underestimation of momentum fluxes in the tropics [*Wright et al.* 2013]. At least concerning GW intermittency, we know that this is the case since *Jewtoukoff et al.* [2013] reported events of GW amplitude near 100 mPa in the tropics whereas the extreme events in *Ern et al.* [2014] are around 15 mPa.

4. Significance and Causes of Intermittency and GW Spectra

4.1. Significance of Intermittency

To illustrate the significance of representing the gravity wavefield as a stochastic process in order to generate GW momentum flux intermittency in our parameterization, we can proceed as in *Lott and Guez* [2013]. In their offline tests with the stochastic scheme linked to convection, the sporadic nature of precipitation translated into fewer events of large GW momentum flux amplitudes, and they showed that the associated GWs broke lower in the atmosphere than when uniform sources were considered. When the parameterization was used in GCM runs, the authors concluded that lower level breaking helped the model to produce

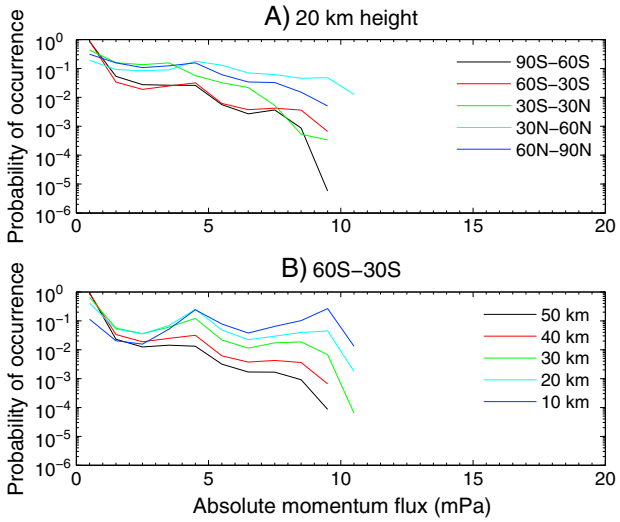

Figure 6. (a) As in Figure 3a and (b) as in Figure 4a but for a launching momentum flux zonally uniformized.

a QBO. Following *Lott and Guez* [2013], offline tests are performed imposing a momentum flux amplitude at the launching level equal to the zonal average at each latitude. Consistently, when the wave sources are sporadic smaller drag is applied in the extratropical higher levels (Figure 5a) than when uniform momentum flux amplitudes are considered (Figure 5b). The drag in the QBO region remains approximately unchanged.

Figure 6 shows the pdfs at different altitudes and latitude bands for the case of uniform momentum flux amplitudes. As compared to the pdfs in Figures 3a and 4a, it is noticeable that there are no large-amplitude events and that the shapes of pdfs do not resemble lognormal distributions. We therefore see that stochastic techniques, when fed by the right statistics, are key to mimic the observed intermittency of GW momentum flux.

This general tendency of our stochastic scheme to produce GWs breaking at lower altitude than more uniform schemes may well be helpful for models. For instance, the QBO currently simulated in GCMs is too weak in amplitude and does not descend to a sufficiently low altitude [e.g., *Giorgetta et al.*, 2006; *Orr et al.*, 2010; *Osprey et al.*, 2013]. Although large-scale Kelvin waves may contribute at least as much as the GWs [*Krismer et al.*, 2013], it is clear that lower level GW breaking can also be helpful. There is some indication that this is indeed the case in *Schirber et al.* [2014], where important aspects of the QBO are improved by relating the GWs to their convective sources. *Lott and Guez* [2013] also found that intermittent waves breaking at quite low altitude helped to decorrelate the QBO and the semiannual oscillation and to produce a QBO with an irregular period.

4.2. Sources of Gravity Wave Intermittency

The results on GW momentum flux intermittency presented in the previous section are consistent with *Hertzog et al.* [2012], who showed that lognormal distributions in extratropical, nonorographic regions are observed in a variety of data sets, including in situ balloons, satellite observations, and high-resolution simulations. They argued that such distributions can simply be due to the dynamical filtering of a wave spectrum propagating through a space-time varying background wind. This naturally questions our assumption of imposing a lognormal distribution on the launched fluxes, i.e., our hypothesis that the lognormality is already present in the GW sources.

To test the sensitivity of momentum flux pdfs to the choice of the launching distribution of background fluxes, we have repeated the offline tests for the Concordiasi period (September 2010 to January 2011) using white noise, as well as Gaussian and lognormal processes, to launch the background flux (i.e., variable G_b in equation (2)). This is shown in Figure 7, where the resulting pdfs are plotted at different heights in the 65°S–50°S latitude band, along with the Concordiasi pdf (at $\sim$ 20 km) for the same region and time interval (note that the GW drags produced by the three different launching flux distributions are reasonably near that shown in Figure 1a). For the cases of white and Gaussian processes (Figures 7a and 7b), the shapes of the pdfs at lower altitudes are far from resembling a lognormal distribution. Interestingly, the pdfs continuously change with height, and at 50 km they clearly share similarities with the observed ones. In fact, a lognormal fit is fairly close to the produced pdf at 50 km. This is especially evident for the lowest values and starts failing for values above 30–40 mPa. For the case of a lognormal process generating the launching flux amplitude (Figure 7c), the pdfs present many similarities at all altitudes with the observed ones. The vertical propagation removes large momentum flux values due to wave dissipation, but the shape of the pdfs is not

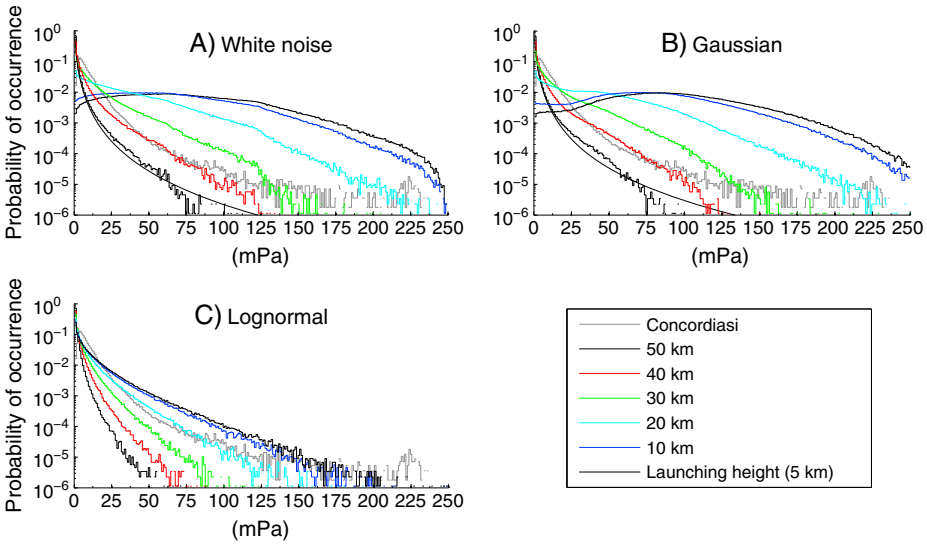

Figure 7. Pdfs of GW absolute momentum fluxes at different altitudes constructed in the 65°S–50°S latitude band from September 2010 to January 2011 and obtained from offline tests of the BCGWD scheme by launching momentum fluxes following (a) a white noise, (b) a Gaussian, and (c) a lognormal distribution. In Figures 7a and 7b, the theoretical lognormal pdf with the same mean and variance as the pdf at 50 km is shown (smooth black curve). The pdf derived from Concordiasi balloons is displayed in all panels (gray).

altered. Comparing with Concordiasi at 20 km, the best performance of the parameterization is undoubtedly achieved using a lognormal source for the background flux.

These results indicate, therefore, that wave dissipation contributes to generate lognormal shapes in momentum flux pdfs, supporting the findings by *Hertzog et al.* [2012], but also that one needs to be at a sufficiently high altitude for this process to be efficient. Our results suggest that imposing a lognormal distribution for the launching flux is mandatory to better represent the fluxes that enter the lower stratosphere (e.g., where they are measured by balloons). This issue raises the question of what causes these distributions in the launching fluxes.

To address this point, we next evaluate the pdfs of two potential GW sources: convection and fronts. For convection, we take squared precipitation, as already used in equation (2). The corresponding pdf is shown in Figure 8a, along with the theoretical lognormal distribution with the same mean and variance. The behavior of the squared precipitation pdf is close to a lognormal, although in general, the theoretical distribution tends to underestimate the values. For fronts, we use recent theoretical results by *Lott et al.* [2010, 2012b], who gave explicit formulae for GW emission from potential vorticity (PV) anomalies in vertically sheared wind. This may be viewed as a proxy for the presence of fronts or for the onset of intense geostrophic

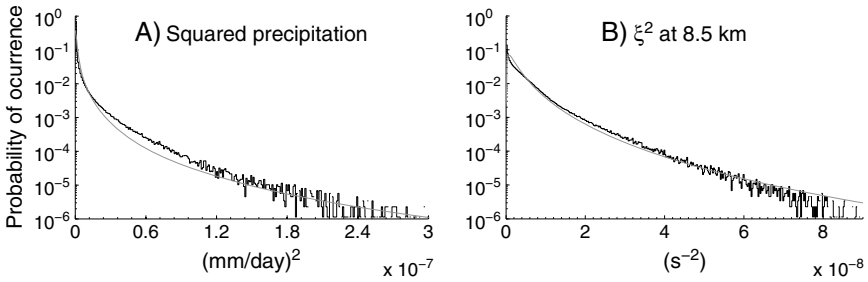

Figure 8. Pdfs of (a) squared precipitation from GPCP data set and (b) squared vorticity at 8.5 km height from ERA-Interim. The pdfs are constructed for the 65°S–50°S latitude band from September 2010 to January 2011. The corresponding theoretical lognormal pdfs with the same mean and variance are shown (gray curve).

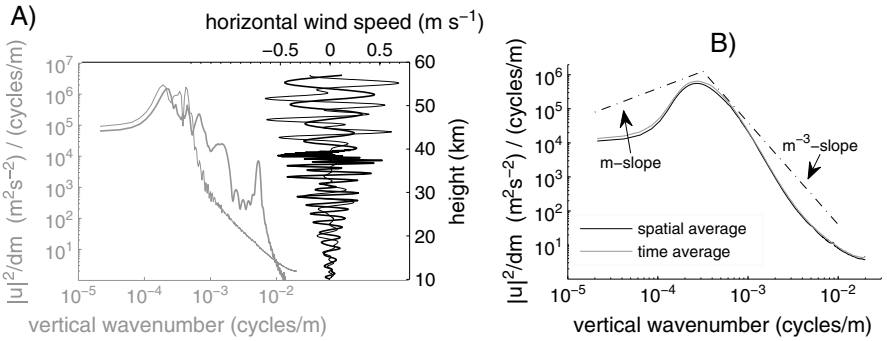

Figure 9. (a) Vertical profiles of horizontal wind perturbation of two realizations of the GW field at two different grid points (bold and light black curves) and the corresponding periodograms (bold and light gray curves). (b) Global energy spectrum of gravity waves obtained averaging a large ensemble of individual periodograms (see text). Dash-dotted lines represent the m and m^{-3} scaling of the observed universal spectrum, as indicated.

adjustment [e.g., *Thorpe and Clough*, 1991]. Whatever is the cause for the presence of the PV anomalies, the above mentioned works derive that the GW amplitude scales linearly with relative vorticity. Based on this, we take the squared vorticity to scale the pdf of GW momentum fluxes. The resulting pdf at 8.5 km is well fitted by a lognormal, slightly overestimating at large values. We have tested other altitudes, also averaged the squared relative vorticity over a range of altitudes, and obtained similar distributions. Although optimizing the relation between emission of GW momentum fluxes and the vorticity diagnostic is beyond the scope of the present study, we have identified here a good candidate to be used as a source of midlatitude GWs in parameterizations.

To conclude, our initial decision of considering a lognormal distribution for the launching background flux is now justified by the fact that GW sources tend to produce such distributions.

4.3. GW Energy Spectra

We compute the energy spectrum of GWs as follows. First, we construct the horizontal velocity perturbation $\vec{u}'_n(x,y,z,t)$ associated to each wave launched at each time step and grid point. From the solution of the vertical structure of the vertical velocity ($\hat{w}_n(z)$ here in equation (1) and equation (4) by *Lott et al.* [2012a]), and using the polarization relation for midfrequency waves under the WKB approximation [e.g., *Fritts and Alexander*, 2003], the following expression can be derived for the horizontal velocity perturbation associated with one GW:

$$\vec{u}'_n(x,y,z,t) = \frac{\vec{k}_n}{\|\vec{k}_n\|}\Re\left\{\left\|\frac{N\hat{w}_n(z)}{\Omega_n(z)}\right\| e^{-i\int_{z_l}^{z} m_n(z')\,dz' + i(\vec{k}_n\vec{x} - i\omega_n t) + i\phi_n}\right\} e^{z/2H}, \tag{4}$$

where ϕ_n is a phase factor that does not need to be estimated to compute the GWs drag and the vertical wind amplitude $\|\hat{w}_n(z)\|$ can be related to the E-P flux by using WKB polarization relations:

$$\|\hat{w}_n(z)\|^2 = \frac{2}{\rho_r}\frac{\|\vec{k}_n\|}{|m_n(z)|}\|\vec{F}_n(z)\|. \tag{5}$$

Both the wind amplitude and the wave phase are computed at every reanalysis vertical level, where the parameterization provides $m_n(z)$, $|\vec{k}_n|$ and $|\vec{F}_n(z)|$. Next, we linearly interpolate $\|N\hat{w}_n/\Omega_n\|$ and the wave phase in the vertical from the reanalysis vertical resolution to a 25 m vertical spacing. Then we perform a Fourier transform on the resulting $u'_n(z)$ in the vertical at a given location and time ($x = x_0$, $y = y_0$, $t = t_0$) and obtain individual periodograms for each monochromatic wave. Note that we could choose here the phase ϕ_n and locations (x, y, t) randomly, but this would not affect the individual periodogram. Finally, the energy spectrum is obtained by averaging a large ensemble of such individual periodograms.

Figure 9a shows the vertical profile of horizontal velocity associated with one realization of our wavefield (bold black curve), $u' = \sum_1^4 C_n u'_n$ at a given horizontal location and choosing the phase randomly (this choice does not influence the results). We see a wavefield made of perturbations with amplitude near and below 1 m/s, consistent with what is routinely observed in vertical soundings [*Scavuzzo et al.*, 1998;

Moldovan et al., 2002]. It is also a good illustrative example of the GWs we parameterized: made of stationary monochromatic GWs, our disturbance field extends over the entire atmosphere. In some regions, for instance, below 40 km, a certain wave with quite a short vertical wavelength dominates before being absorbed at around 40 km, and above it another wave dominates. By imposing monochromatic waves, our scheme exaggerates the observational fact that at a given place, narrowband wave packets dominate the signal, and it is finally the dynamical filtering of the waves which causes one perturbation at a given altitude to dominate the others. Another example is given by the thin black curve in Figure 9a for illustration. The disturbance is of much smaller amplitude below 40 km, consistent with our stochastic choice of the launching amplitude and wave parameters. The dominant vertical wavelength is also larger in many places, because the chosen phase speed is larger than in the previous case. Figure 9a also shows the sum of the four periodograms associated with the wavefields presented (bold and thin gray curves). They are quite narrowbanded with strong peaks around $2 \cdot 10^{-4}$ cycles/m and secondary peaks at $4 \cdot 10^{-4}$, 10^{-3}, and $5 \cdot 10^{-3}$ cycles/m. Overall, the behavior of the spectra before large ensemble averaging is consistent with the fact that we perform the Fourier analysis of only few random realizations with rather well-defined oscillations in the vertical.

We next compute large ensemble averages of the individual periodograms and obtain the energy spectrum shown in Figure 9b. Two types of average are plotted, a spatial average over the whole globe for a particular day in October 2010 (black curve), and a time average from September 2010 to January 2011 for a grid point at 60°S. Also, shown in Figure 9b is the well-known m^{-3} slope derived from radar and radiosondes measurements during the 1980s [e.g., *VanZandt*, 1982; *Fritts et al.*, 1988]. This property, reasonably well explained by different theories of saturated wave spectra [e.g., *Dewan and Good*, 1986; *Smith et al.*, 1987; *Fritts*, 1989; *Fritts and Lu*, 1993], is on the basis of the globally spectral parameterizations of GW drag. The spectral slope for wave numbers ($m \geq 3 \cdot 10^{-4}$ m^{-1}) is not far from the m^{-3} dependence, but it gets steeper for large wave numbers ($10^{-3} < m < 5 \cdot 10^{-3}$ m^{-1}). Combining equations (3) and (5), it can be derived that the saturated energy spectrum in the BCGWD scheme $\|u_s\|^2 \mathrm{d}m^{-1}$ is proportional to $\sim m^{-2}\mathrm{d}m^{-1} \sim m^{-3}$. To explain the departures from this dependence it should be taken into account that critical level filtering mostly affects waves with large wave numbers due to Doppler shifting near a critical line (as illustrated in Figure 9a), providing extra GW energy dissipation.

The unsaturated part of the spectrum (i.e., small vertical wave numbers) in the above mentioned observations presents a $\sim m$ scaling and has been represented by a dashed line in Figure 9b. It clearly differs from the BCGWD scheme, but this is expected. The unsaturated part of the spectrum is directly influenced by the spectrum of GWs launched in the scheme, since neither wave breaking nor critical levels affect the small vertical wave numbers involved. Combining equations (2) and (5), it can be shown that the launched convective GW spectrum is proportional to m^4, and the launched background GW spectrum is proportional to m. Therefore, the unsaturated part of the spectrum is a combination of these two dependencies in the BCGWD scheme. We could have forced the launched fluxes to follow a m slope, but in the absence of theoretical justification for this, we have preferred not to do so.

Overall, we can conclude that the so-called observed universal spectrum can roughly be obtained with a multiwave stochastic scheme as a superposition of individual periodograms.

5. Summary and Concluding Remarks

Recent observational studies highlight that the GW field is highly intermittent [e.g., *Hertzog et al.*, 2012; *Wright et al.*, 2013]. This has implications for GW parameterizations in GCMs, since a given averaged momentum flux carried by a large number of small-amplitude GWs will produce a drag at much higher altitudes than that produced by the same averaged flux carried by a small number of high-amplitude GWs. The goal of the present study has been to examine GW momentum flux intermittency parameterized by the stochastic multiwave scheme recently proposed by *Lott et al.* [2012a] and *Lott and Guez* [2013]. To that aim, we have conducted offline experiments using ERA-Interim wind and temperature fields and precipitation from GPCP data set, and considered both convective and random background sources, the latter accounting for other nonspecified sources active in midlatitudes, such as fronts. The offline tests have been performed with the limiting constraint that the produced GW drag compares well with that produced by offline runs of the operational scheme used in the LMDz GCM (the *Hines* [1997] scheme).

First, we have studied the intermittency predicted by the parameterization by examining the pdfs of absolute GW momentum fluxes. The scheme parameters have been adjusted in such a way that the pdfs at 20 km over the 65°S–50°S latitude band compare well with in situ observations of balloon flights during the Concordiasi field campaign in the austral spring of 2010. The distributions of GW momentum fluxes have lognormal-like shapes, characterized by long tails that signal the presence of sporadic high-amplitude events. We have described the variations of momentum flux intermittency with height, latitude, and season as produced by our offline tests. At a given altitude, the pdfs present longer tails in the extratropical winter, and they change their shape toward shorter tails as we go up in the atmosphere. No significant seasonal modulation is present in the tropics. These results qualitatively agree with those derived from the HIRDLS instrument on NASA's Aura satellite shown by *Wright et al.* [2013], especially in the extratropics. Besides, our results suggest self-similarity: the 90th and 99th percentiles of momentum flux distributions approximately explain the same proportion of the total flux at different altitudes. This feature has been recently noted by *Hertzog et al.* [2012] in high-resolution numerical simulations. We have also shown that it is beneficial to constrain the GW drag parameterizations using observational characteristics of GW momentum flux intermittency. In this regard, it would be interesting to include diagnostics of momentum flux intermittency in global comparisons between momentum fluxes measured in observations and modeled in GCMs [*Geller et al.*, 2013].

Next, the causes of the observed lognormal pdfs have been analyzed using our stochastic scheme. We find that dynamical filtering by the winds modifies the shape of the launched pdfs toward a lognormal, as suggested by previous studies [e.g., *Hertzog et al.*, 2012]. However, the pdfs become lognormal at very high altitudes (around 50 km), and we are forced to choose the launching momentum flux out of a lognormal distribution in order to obtain pdfs comparable to balloons observations in the lower stratosphere. This implies that GW sources may have lognormal distributions, and in fact, we have demonstrated that the pdfs of two potential sources, convection and fronts, fairly follow such a distribution.

Finally, we have shown that the well-known universal spectrum of GWs can be obtained by superposition of individual narrowbanded periodograms produced by our stochastic, multiwave scheme. This has been achieved despite some strong simplifications made in this kind of parameterizations, such as assuming that each GW behaves independently from the others. To some extent, this result reconciles the apparently contrasting approaches used to parameterize nonorographic GWs in general circulation models, namely the globally spectral schemes and the multiwave schemes. A clear advantage of the stochastic multiwave formulation used in the present study is that GWs can be easily related to their sources. As done by *Lott and Guez* [2013] with convection, it is interesting to go one step forward and link the GWs to vorticity anomalies in order to parameterize GWs produced by fronts, as suggested by *Lott et al.* [2010, 2012b]. Such a study is subject of ongoing work.

Acknowledgments

The authors thank three anonymous reviewers for their insightful comments and V. Jewtoukoff for useful discussions. This work was supported by the European Commission's Seventh Framework Programme, under the project EMBRACE (grant agreement 282672) and by the French ANR project Stradyvarius. GPCP precipitation data are provided by the NOAA/OAR/ESRL PSD, Boulder (CO), USA, from their website at http://www.esrl.noaa.gov/psd/. Concordiasi was built by an international scientific group and is currently supported by the following agencies: Météo-France, CNES, IPEV, PNRA, CNRS/INSU, NSF, NCAR, Concordia consortium, University of Wyoming, and Purdue University. ECMWF also contributes to the project through computer resources and support, and scientific expertise. The two operational polar agencies PNRA and IPEV are thanked for their support at Concordia station. Concordiasi is part of the THORPEX-IPY cluster within the International Polar Year effort.

References

Adler, R. F., et al. (2003), The version 2 global precipitation climatology project (GPCP) monthly precipitation analysis (1979–present), *J. Hydrometeorol.*, *4*, 1147–1167.

Alexander, M. J., and T. J. Dunkerton (1999), A spectral parameterization of mean-flow forcing due to breaking gravity waves, *J. Atmos. Sci.*, *56*, 4167–4182.

Alexander, M. J., et al. (2010), Recent developments in gravity-wave effects in climate models and the global distribution of gravity-wave momentum flux from observations and models, *Q. J. R. Meteorol. Soc.*, *136*(650), 1103–1124, doi:10.1002/qj.637.

Baumgaertner, A. J. G., and A. J. McDonald (2007), A gravity wave climatology for Antarctica compiled from Challenging Minisatellite Payload/Global Positioning System (CHAMP/GPS) radio occultations, *J. Geophys. Res.*, *112*, D05103, doi:10.1029/2006JD007504.

Boccara, G., A. Hertzog, R. A. Vincent, and F. Vial (2008), Estimation of gravity wave momentum flux and phase speeds from quasi-Lagrangian stratospheric balloon flights. Part I: Theory and simulations, *J. Atmos. Sci.*, *65*, 3042–3055, doi:10.1175/2008JAS2709.1.

Dee, D. P., et al. (2011), The ERA-interim reanalysis: Configuration and performance of the data assimilation system, *Q. J. R. Meteorol. Soc.*, *137*(1), 553–597, doi:10.1002/qj.828.

Dewan, E. M., and R. E. Good (1986), Saturation and the "universal" spectrum for vertical profiles of horizontal scalar winds in the atmosphere, *J. Geophys. Res.*, *91*(D2), 2742–2748.

Eckermann, S. D. (2011), Explicitly stochastic parameterization of nonorographic gravity wave drag, *J. Atmos. Sci*, *68*, 1749–1765, doi:10.1175/2011JAS3684.1.

Ern, M., P. Preusse, J. C. Gille, C. L. Hepplewhite, M. G. Mlynczak, J. M. Russell III, and M. Riese (2011), Implications for atmospheric dynamics derived from global observations of gravity wave momentum flux in stratosphere and mesosphere, *J. Geophys. Res.*, *116*, D19107, doi:10.1029/2011JD015821.

Ern, M., F. Ploeger, P. Preusse, J. C. Gille, L. J. Gray, S. Kalisch, M. G. Mlynczak, J. M. Russell III, and M. Riese (2014), Interaction of gravity waves with the QBO: A satellite perspective, *J. Geophys. Res. Atmos.*, *119*, 2329–2355, doi:10.1002/2013JD020731.

Fritts, D. C. (1989), A review of gravity wave saturation processes, effects, and variability in the middle atmosphere, *Pure Appl. Geophys.*, *130*, 343–371.

Fritts, D. C., and M. J. Alexander (2003), Gravity wave dynamics and effects in the middle atmosphere, *Rev. Geophys.*, *41*(1), 1003, doi:10.1029/2001RG000106.
Fritts, D. C., and W. Lu (1993), Spectral estimates and gravity wave energy and momentum fluxes. Part II: Parameterization of wave forcing and variability, *J. Atmos. Sci.*, *50*, 3695–3713.
Fritts, D. C., T. Tsuda, T. Sato, S. Fukao, and S. Kato (1988), Observational evidence of a saturated gravity wave spectrum in the troposphere and lower stratosphere, *J. Atmos. Sci.*, *45*(12), 1741–1759.
Fritts, D. C., S. L. Vadas, and Y. Yamada (2002), An estimate of strong local body forcing and gravity wave radiation based on OH airglow and meteor radar observations, *Geophys. Res. Lett.*, *29*(10), 71-1–71-4, doi:10.1029/2001GL013753.
Fritts, D. C., D. Janches, W. K. Hocking, N. J. Mitchell, and M. J. Taylor (2012), Assessment of gravity wave momentum flux measurement capabilities by meteor radars having different transmitter power and antenna configurations, *J. Geophys. Res.*, *117*, D10108, doi:10.1029/2011JD017174.
Geller, M. A., et al. (2013), A comparison between gravity wave momentum fluxes in observations and climate models, *J. Clim.*, *26*, 6383–6405, doi:10.1175/JCLI-D-12-00545.1.
Giorgetta, M. A., E. Manzini, E. Roeckner, M. Esch, and L. Bengston (2006), Climatology and forcing of the quasi-biennial oscillation in the MAECHAM5 model, *J. Clim.*, *19*, 3882–3901, doi:10.1175/JCLI3830.1.
Hertzog, A., et al. (2007), Stratéole/Vorcore—Long-duration superpressure balloons to study the Antarctic lower stratosphere during the 2005 winter, *J. Atmos. Oceanic Technol.*, *24*, 2048–2061, doi:10.1175/2007JTECHA948.1.
Hertzog, A., G. Boccara, R. A. Vincent, F. Vial, and P. Cocquerez (2008), Estimation of gravity wave momentum flux and phase speeds from quasi-Lagrangian stratospheric balloon flights. Part II: Results from the Vorcore campaign in Antarctica, *J. Atmos. Sci.*, *65*, 3056–3070, doi:10.1175/2008JAS2710.1.
Hertzog, A., M. J. Alexander, and R. Plougonven (2012), On the intermittency of gravity wave momentum flux in the stratosphere, *J. Atmos. Sci.*, *69*, 3433–3448, doi:10.1175/JAS-D-12-09.1.
Hines, C. O. (1997), Doppler spread parameterization of gravity wave momentum deposition in the middle atmosphere. Part 2: Broad and quasi-monochromatic spectra and implementation, *J. Atmos. Sol. Terr. Phys.*, *59*, 387–400.
Holton, J. R. (1983), The influence of gravity wave breaking on the general circulation of the middle atmosphere, *J. Atmos. Sci.*, *40*, 2497–2507.
Hoffmann, L., X. Xue, and M. J. Alexander (2013), A global view of stratospheric gravity wave hotspots located with Atmospheric Infrared Sounder observations, *J. Geophys. Res. Atmos.*, *118*, 416–434, doi:10.1029/2012JD018658.
Jewtoukoff, V., R. Plougonven, and A. Hertzog (2013), Gravity waves generated by deep tropical convection: Estimates from balloon observations and mesoscale simulations, *J. Geophys. Res. Atmos.*, *118*, 9690–9707, doi:10.1002/jgrd.50781.
Krismer, T., M. A. Giorgetta, and M. Esch (2013), Seasonal aspects of the quasi-biennial oscillation in the Max Planck Institute Earth System Model and ERA-40, *J. Adv. Model. Earth Syst.*, *5*, 406–421, doi:10.1002/jame.20024.
Lindzen, R. S. (1981), Turbulence and stress owing to gravity wave and tidal breakdown, *J. Geophys. Res.*, *86*, 9707–9714, doi:10.1002/jgrd.50705.
Lindzen, R. S., and J. R. Holton (1968), A theory of the quasi-biennial oscillation, *J. Atmos. Sci.*, *25*, 1095–1107.
Lott, F., and L. Guez (2013), A stochastic parameterization of the gravity waves due to convection and its impact on the equatorial stratosphere, *J. Geophys. Res. Atmos.*, *118*, 8897–8909, doi:10.1002/jgrd.50705.
Lott, F., L. Fairhead, F. Hourdin, and P. Levan (2005), The stratospheric version of LMDz: Dynamical climatologies, Arctic Oscillation, and impact on the surface climate, *Clim. Dyn.*, *25*, 851–868, doi:10.1007/s00382-005-0064-x.
Lott, F., R. Plougonven, and J. Vanneste (2010), Gravity waves generated by sheared potential vorticity anomalies, *J. Atmos. Sci.*, *67*, 157–170, doi:10.1175/2009JAS3134.1.
Lott, F., L. Guez, and P. Maury (2012a), A stochastic parameterization of non-orographic gravity waves: Formalism and impact on the equatorial stratosphere, *Geophys. Res. Lett.*, *39*, L06807, doi:10.1029/2012GL051001.
Lott, F., R. Plougonven, and J. Vanneste (2012b), Gravity waves generated by a sheared three-dimensional potential vorticity anomalies, *J. Atmos. Sci.*, *69*, 2134–2151, doi:10.1175/JAS-D-11-0296.1.
Moldovan, H., F. Lott, and H. Teitelbaum (2002), Wave breaking and critical levels for propagating inertio-gravity waves in the lower stratosphere, *Q. J. R. Meteorol. Soc.*, *128*, 713–732.
Orr, A., P. Bechtold, J. Scinocca, M. Ern, and M. Janiskova (2010), Improved middle atmosphere climate and forecasts in the ECMWF model through a nonorographic gravity wave drag parameterization, *J. Clim.*, *23*, 5905–5926, doi:10.1175/2010JCLI3490.1.
Osprey, S. M., L. J. Gray, S. C. Hardiman, N. Butchart, and T. J. Hinton (2013), Stratospheric variability in twentieth-century CMIP5 simulations of the Met Office climate model: High top versus low top, *J. Clim.*, *26*, 1595–1606, doi:10.1175/JCLI-D-12-00147.1.
Plougonven, R., A. Hertzog, and H. Teitelbaum (2008), Observations and simulations of a large amplitude mountain wave breaking over the Antarctic Peninsula, *J. Geophys. Res.*, *113*, D16113, doi:10.1029/2007JD009739.
Plougonven, R., A. Hertzog, and L. Guez (2013), Gravity waves over Antarctica and the Southern Ocean: Consistent momentum fluxes in mesoscale simulations and stratospheric balloon observations, *Q. J. R. Meteorol. Soc.*, *139*(670), 101–118, doi:10.1002/qj.1965.
Rabier, F., et al. (2010), The CONCORDIASI project in Antarctica, *Bull. Am. Meteorol. Soc.*, *91*, 69–86, doi:10.1175/2009BAMS2764.1.
Richter, J. H., F. Sassi, and R. R. Garcia (2010), Toward a physically based gravity wave source parameterization in a general circulation model, *J. Atmos. Sci.*, *67*, 136–156, doi:10.1175/2009JAS3112.1.
Scavuzzo, M., C. Lamfri, H. Teitelbaum, and F. Lott (1998), A study of the low frequency inertio-gravity waves observed during PYREX, *J. Geophys. Res.*, *103*(D2), 1747–1758.
Schirber, S., E. Manzini, and M. J. Alexander (2014), A convection-based gravity wave parameterization in a general circulation model: Implementation and improvements on the QBO, *J. Adv. Model. Earth Syst.*, *6*, 264–279, doi:10.1002/2013MS000286.
Scinocca, J. F. (2003), An accurate spectral nonorographic gravity wave drag parameterization for general circulation models, *J. Atmos. Sci.*, *60*, 667–682.
Smith, S. A., D. C. Fritts, and T. E. VanZandt (1987), Evidence for a saturated spectrum of atmospheric gravity waves, *J. Atmos. Sci.*, *44*, 1404–1410.
Song, I.-S., and H.-Y. Chun (2008), A Lagrangian spectral parameterization of gravity wave drag induced by cumulus convection, *J. Atmos. Sci.*, *65*, 1204–1224, doi:10.1175/2007JAS2369.1.
Thorpe, A. J., and S. A. Clough (1991), Mesoscale dynamics of cold fronts: Structures described by dropsoundings in FRONTS 87, *Q. J. R. Meteorol. Soc.*, *117*, 903–941.
VanZandt, T. E. (1982), A universal spectrum of buoyancy waves in the atmosphere, *Geophys. Res. Lett.*, *9*, 575–578.
Warner, C. D., and M. E. McIntyre (1996), On the propagation and dissipation of gravity wave spectra through a realistic middle atmosphere, *J. Atmos. Sci.*, *53*, 3213–3235.

Watanabe, S., Y. Kawatani, Y. Tomikawa, K. Miyazaki, M. Takahashi, and K. Sato (2008), General aspects of a T213L256 middle atmosphere general circulation model, *J. Geophys. Res.*, *113*, D12110, doi:10.1029/2008JD010026.

Wright, C. J., S. M. Osprey, and J. C. Gille (2013), Global observations of gravity wave intermittency and its impact on the observed momentum flux morphology, *J. Geophys. Res. Atmos.*, *118*, 10,980–10,993, doi:10.1002/jgrd.50869.